SECOND ORDER SLIDING MODE CONTROL OF A DUAL-ROTOR WIND TURBINE SYSTEM BY EMPLOYING A MATRIX CONVERTER

Adil. YAHDOU **Boualem. HEMICI**
Process Control Laboratory, Automatic Department, National Polytechnic School, El Harache, Algeria.
yahdou10h@yahoo.fr bhemici@yahoo.fr

Zinelabidine. BOUDJEMA
LGEER Laboratory, Electrical Engineering Department, University of Chlef, Algeria.
boudjemaa1983@yahoo.fr

Abstract: *This paper deals with a variable speed device to produce electrical energy on a power network, based on a doubly-fed induction generator (DFIG) fed by a matrix converter and driven by dual rotor wind turbine. The scientific literature indicates that a dual-rotor wind turbine (DRWT) system could extract additional 20-30% power compared to a single rotor wind turbine (SRWT) system from the same wind stream. In the first place, we study the aerodynamic model of DRWT. In the second place, we carried out a study of modelling on the matrix converter controlled by the Venturini modulation technique and we developed a model of the doubly fed induction generator. In order to control the power flowing between the stator of the DFIG and the power network, a control law is synthesized using two types of controllers: PI and second order sliding mode (SOSMC). Their respective performances are compared in terms of power reference tracking, response to sudden speed variations, sensitivity to perturbations and robustness against machine parameters variations.*

Key words: *Doubly fed induction generator, dual rotor wind turbine, matrix converter, PI controller, second order sliding mode.*

1. Introduction

The horizontal axis wind turbine, which has a single rotor wind turbine and three blades, has been widely used as the conventional type of wind turbines. However, various other types of wind turbines have been proposed for improvement of power efficiency and suitability for low wind speeds [1,2].

The dual rotor wind turbine has been proposed as a new design for improvement of power efficiency, as shown in Figure 1. Its configuration consists of two rotors rotating in opposite directions on the same axis. According to the momentum theory by Newman [3], the ideal maximum power coefficient of a wind turbine having a single rotor is about 59% [4], but that of a wind turbine having two rotors is about 64%, which is about 5% improvement. Based on this result, several experimental studies on the DRWT have been carried out to ultimately extract more power from the wind.

Robust control power used in this paper is the second order sliding mode which is a particular mode of functioning of systems with variable structure. The "higher order sliding mode" control approach has been recently proposed [5,6,7] and developed as a generalization of the classical first order sliding mode theory. In higher order sliding mode control the selected sliding variable has relative degree greater than one with respect to the control. The discontinuous control signal acts on the higher derivatives of s to enforce a sliding motion on $s = 0$. For example, in second order sliding mode, the control affects of the second derivative of $s = 0$. Higher order sliding mode control provides a natural solution to avoid the chattering effect, shows robustness against various kinds of uncertainties such as external disturbances and measurement errors (as the standard sliding mode control [8]) and provides a higher order precision. The main results concern the second order sliding mode control [9], even if sliding mode strategies of order higher than two have been proposed for nonlinear systems [10,11,12].

This paper is devised in six sections as follows: in section 2 we briefly review the system modeling. In section 3 we present the control of active and reactive powers of the DFIG using the SOSMC and vector control using PI controller. In section 4, we propose to compare the mechanical power extracted from a single and dual rotor wind turbine and then the two controllers are compared by simulation in terms of power reference tracking, sensitivity to the speed variation and robustness against machine parameters variations. Finally, in section 5 the main conclusions of the work are drawn.

2. The DRWT model

Aerodynamic model of DRWT is different from SRWT to some extent. Since the wind which is flowing through the main turbine in DRWT is disturbed by the auxiliary turbine, then stream tube effect must be included in the aerodynamic torque calculations for

DRWT. Through (1) & (2) aerodynamic torque of the main and auxiliary turbines are introduced by the blades is as follows:

$$T_M = 0.5\rho.\pi.R_M{}^5.C_p.\omega_M^2 / \lambda_M^3 \quad (1)$$

$$T_A = 0.5\rho.\pi.R_A{}^5.C_p.\omega_A^2 / \lambda_A^3 \quad (2)$$

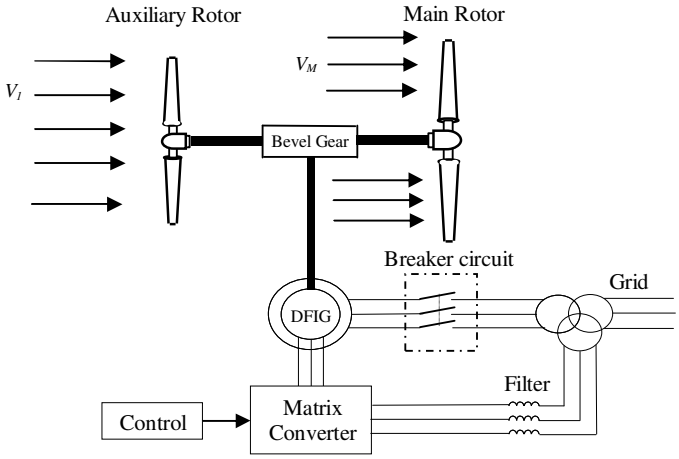

Fig. 1. Block diagram of DRWT with a DFIG fed by matrix converter.

With R_M , R_A : blade radius of the main and auxiliary turbines, λ_M λ_A : the tip speed ratio of the main and auxiliary turbines, ρ : the air density and ω_M, ω_A the mechanical speed of the main and auxiliary rotors. *Cp* can be calculated as follows [13]:

$$C_p(\lambda,\beta) = 0.517(\frac{116}{\lambda_i} - 0.4\beta - 5).e^{\frac{-21}{\lambda_i}} + 0.0068\lambda$$

$$\frac{1}{\lambda_i} = \frac{1}{\lambda + 0.08\beta} - \frac{0.035}{\beta^3 + 1} \quad (3)$$

With β is pitch angle.

Same method can be followed for main and auxiliary turbines. Tip speed ratios for the main and auxiliary turbines are calculated through (4) and (5), respectively.

$$\lambda_A = \omega_A.R_A / V_1 \quad (4)$$

$$\lambda_M = \omega_M.R_M / V_M \quad (5)$$

Where V_1 is the wind speed on auxiliary wind turbine and V_M is the speed of the unified wind on main turbine. So, the essential element for calculating the tip speed ratio is wind speed on the main and auxiliary turbines. Obtaining the wind speed on auxiliary turbine is straight forward. However, calculation of wind speed on main turbine requires further investigation. Based on the (6), it is possible to estimate the amount of the wind speed at any point between the auxiliary and main blades.

$$V_x = V_1(1 - \frac{1-\sqrt{1-C_T}}{2}(1 + \frac{2.x}{\sqrt{1+4.x^2}})) \quad (6)$$

With x the non-dimensional distance from the auxiliary rotor disk, V_x the velocity of the disturbed wind between rotors at point x and C_T the trust coefficient which is taken to be 0.9. So, with respect to x=15, the value of the V_x close to the main rotor is computable (rotors are located 15 meters apart from each other) [14].

3. Matrix converter modeling

The matrix converter performs the power conversion directly from AC to AC without any intermediate dc link. It is very simple in structure and has powerful controllability. The converter consists of a matrix of bi-directional switches linking two independent three-phase systems. Each output line is linked to each input line via a bi-directional switch. Figure 2 shows the basic diagram of a matrix converter [15].

The switching function of a switch S_{mn} in figure 2 is given by:

$$S_{mn} = \begin{cases} 1 & S_{mn} \text{ closed} \\ 0 & S_{mn} \text{ open} \end{cases} \quad m \in \{A,B,C\},\ n \in \{a,b,c\} \quad (7)$$

The mathematical expression that represents the operation of the matrix converter in figure 2 can be written as [16,17] :

$$\begin{bmatrix} V_a \\ V_b \\ V_c \end{bmatrix} = \begin{bmatrix} S_{Aa} & S_{Ab} & S_{Ac} \\ S_{Ba} & S_{Bb} & S_{Bc} \\ S_{Ca} & S_{Cb} & S_{Cc} \end{bmatrix} \cdot \begin{bmatrix} V_A \\ V_B \\ V_C \end{bmatrix} \quad (8)$$

$$\begin{bmatrix} i_A \\ i_B \\ i_C \end{bmatrix} = \begin{bmatrix} S_{Aa} & S_{Ba} & S_{Ca} \\ S_{Ab} & S_{Bb} & S_{Cb} \\ S_{Ac} & S_{Bc} & S_{Cc} \end{bmatrix}^T \cdot \begin{bmatrix} i_a \\ i_b \\ i_c \end{bmatrix} \quad (9)$$

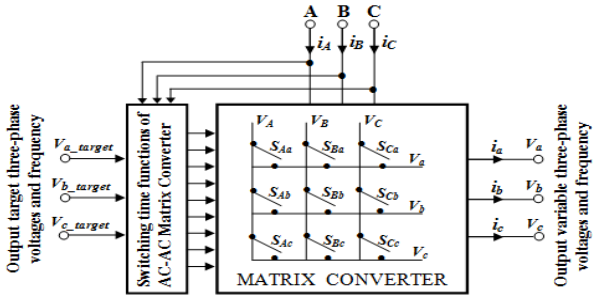

Fig. 2. Schematic representation of the matrix converter.

To determine the behavior of the matrix converter at output frequencies well below the switching frequency, a modulation duty cycle can be defined for each switch.

The input/output relationships of voltages and currents are related to the states of the nine switches and can be expressed as follows :

$$\begin{bmatrix} V_a \\ V_b \\ V_c \end{bmatrix} = \begin{bmatrix} k_{Aa} & k_{Ab} & k_{Ac} \\ k_{Ba} & k_{Bb} & k_{Bc} \\ k_{Ca} & k_{Cb} & k_{Cc} \end{bmatrix} \cdot \begin{bmatrix} V_A \\ V_B \\ V_C \end{bmatrix} \quad (10)$$

$$\begin{bmatrix} i_A \\ i_B \\ i_C \end{bmatrix} = \begin{bmatrix} k_{Aa} & k_{Ba} & k_{Ca} \\ k_{Ab} & k_{Bb} & k_{Cb} \\ k_{Ac} & k_{Bc} & k_{Cc} \end{bmatrix}^T \cdot \begin{bmatrix} i_a \\ i_b \\ i_c \end{bmatrix} \quad (11)$$

With :

$$0 \le k_{mn} \le 1, \quad m = A, B, C, \quad n = a, b, c \quad (12)$$

The variables k_{mn} are the duty cycles of the nine switches S_{mn} and can be represented by the duty-cycle matrix k. In order to prevent a short circuit on the input side and ensure uninterrupted load current flow, these duty cycles must satisfy the three following constraint conditions :

$$k_{Aa} + k_{Ab} + k_{Ac} = 1 \quad (13)$$
$$k_{Ba} + k_{Bb} + k_{Bc} = 1 \quad (14)$$
$$k_{Ca} + k_{Cb} + k_{Cc} = 1 \quad (15)$$

The high-frequency synthesis technique introduced by Venturini (1980) and Alesina and Venturini (1988), allows a control of the S_{mn} switches so that the low frequency parts of the synthesized output voltages (V_a, V_b and V_c) and the input currents (i_A, i_B and i_C) are purely sinusoidal with the prescribed values of the output frequency, the input frequency, the displacement factor and the input amplitude.

Where θ: is the initial phase angle. The output voltage is given by :

$$\begin{bmatrix} V_a \\ V_b \\ V_c \end{bmatrix} = \begin{bmatrix} 1+2\delta\cos\alpha & 1+2\delta\cos(\alpha-\frac{2\pi}{3}) & 1+2\delta\cos(\alpha-\frac{4\pi}{3}) \\ 1+2\delta\cos(\alpha-\frac{4\pi}{3}) & 1+2\delta\cos\alpha & 1+2\delta\cos(\alpha-\frac{2\pi}{3}) \\ 1+2\delta\cos(\alpha-\frac{2\pi}{3}) & 1+2\delta\cos(\alpha-\frac{4\pi}{3}) & 1+2\delta\cos\alpha \end{bmatrix} \cdot \begin{bmatrix} V_A \\ V_B \\ V_C \end{bmatrix} \quad (16)$$

Where : $\begin{cases} \alpha = \omega_m + \theta \\ \omega_m = \omega_{output} - \omega_{input} \end{cases}$

The running matrix converter with Venturini algorithm generates at the output a three-phases sinusoidal voltages system having in that order pulsation ω_m, a phase angle θ and amplitude $\delta.V_s$ ($0 < \delta <$ 0.866 with modulation of the neural) [18].

4. Doubly fed induction generator modeling

A DFIG is used to produce electrical power at constant frequency whatever wind and shaft speed conditions. We used the classical d-q modeling of the induction generator in the Park reference frame [19].

$$\begin{cases} V_{ds} = R_s I_{ds} + \frac{d}{dt}\psi_{ds} - \omega_s \psi_{qs} \\ V_{qs} = R_s I_{qs} + \frac{d}{dt}\psi_{qs} + \omega_s \psi_{ds} \\ V_{dr} = R_r I_{dr} + \frac{d}{dt}\psi_{dr} - \omega_r \psi_{qr} \\ V_{qr} = R_r I_{qr} + \frac{d}{dt}\psi_{qr} + \omega_r \psi_{dr} \end{cases}, \begin{cases} \psi_{ds} = L_s I_{ds} + M I_{dr} \\ \psi_{qs} = L_s I_{qs} + M I_{qr} \\ \psi_{dr} = L_r I_{dr} + M I_{ds} \\ \psi_{qr} = L_r I_{qr} + M I_{qs} \\ g = (\omega_s - \omega)/\omega_s \end{cases} \quad (17)$$

V_{ds}, V_{qs}, V_{dr}, V_{qr} are the statoric and rotoric voltages in the d-q reference frame.

I_{ds}, I_{qs},I_{dr}, I_{qr} are the statoric and rotoric currents in the d-q reference frame.

ψ_{ds}, ψ_{qs}, ψ_{dr} and ψ_{qr} are statoric and rotoric flux in the d-q reference frame.

The stator and rotor angular velocities are linked by the following relation : $\omega_s = \omega + \omega_r$.

The mechanical equation is :

$$T_{em} = T_r + J\frac{d\Omega}{dt} + f\Omega \quad (18)$$

T_{em} is the electromagnetic torque, T_r the resistant torque, f the viscous torque coefficient, Ω the mechanical rotation speed and J the global inertia.

The electromagnetic torque depends on d-q flux and current :

$$T_{em} = p\frac{M}{L_s}(\psi_{ds} I_{qr} - \psi_{qs} I_{dr}) \quad (19)$$

In order to easily control the production of electricity

by the wind turbine, we will carry out an independent control of active and reactive powers by orientation of flux, rotor currents will be related directly to the stator active and reactive power. An adapted control of these currents will thus permit to control the power exchanged between the stator and the grid. If the stator flux is linked to the d-axis of the frame we have :

$$\psi_{ds} = \psi_s \quad \text{and} \quad \psi_{qs} = 0 \tag{20}$$

The electromagnetic torque can then be expressed as follows :

$$T_{em} = p\frac{M}{L_s} I_{qr}\psi_{ds} \tag{21}$$

The grid is assumed to be stable and consequently ψ_{ds} constant. By neglecting the statoric resistor of the DFIG, we obtained :

$$\psi_s = \frac{V_s}{\omega_s} \tag{22}$$

Where V_s: is the rms value of the grid voltage. The active and reactive powers of the DFIG can be expressed by :

$$\begin{cases} P_s = V_s I_{qs} \\ Q_s = V_s I_{ds} \end{cases} \tag{23}$$

Or from the rotoric currents by :

$$\begin{cases} P_s = -V_s \dfrac{M}{L_s} I_{qr} \\ Q_s = \dfrac{V_s^2}{\omega_s L_s} - \dfrac{V_s M}{L_s} I_{dr} \end{cases} \tag{24}$$

Posing $\sigma = 1 - \dfrac{M^2}{L_s L_r}$. Rotor voltages can be expressed:

$$\begin{cases} V_{dr} = R_r I_{dr} + \sigma L_r \dfrac{dI_{dr}}{dt} - g\omega_s \sigma L_r I_{qr} \\ V_{qr} = R_r I_{qr} + \sigma L_r \dfrac{dI_{qr}}{dt} + g\omega_s \sigma L_r I_{dr} + g\dfrac{MV_s}{L_s} \end{cases} \tag{25}$$

We have $s = d/dt$: Laplace operator, the equation 25 becomes:

$$\begin{cases} V_{dr} = R_r I_{dr} + s\sigma L_r I_{dr} - g\omega_s \sigma L_r I_{qr} \\ V_{qr} = R_r I_{qr} + s\sigma L_r I_{qr} + g\omega_s \sigma L_r I_{dr} + g\dfrac{MV_s}{L_s} \end{cases} \tag{26}$$

The resulting block diagram of the DFIG is presented in figure 3.

The third term of equation system 25, which constitutes cross-coupling terms, can be neglected the stator flux.

By choosing a reference frame linked to the stator because of their small influence. These terms can be compensated by an adequate synthesis of the regulators in the control loops. Figure 4 shows a part of our system corrected by the PI controller whose transfer function is of the form $K_p+(K_i/s)$. We choose the method of compensation pole for the synthesis of controllers.

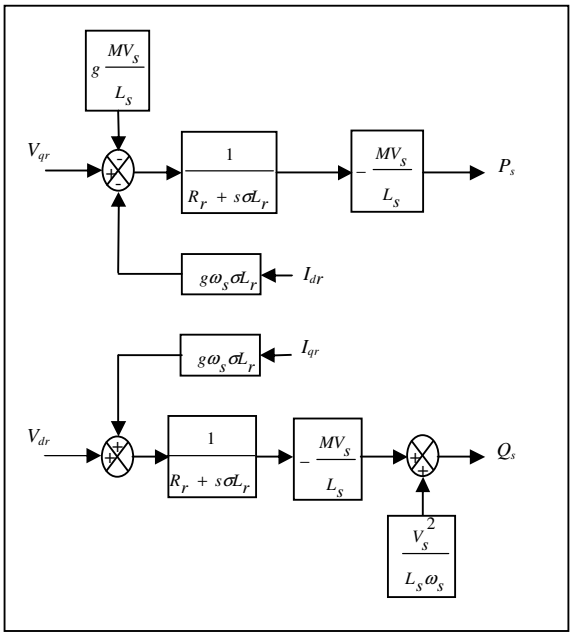

Fig. 3. Diagram of the DFIG.

5. PI controller synthesis

This controller is simple to elaborate. Figure 5 shows the block diagram of the system implemented with this controller. The terms K_p and K_i represent respectively the proportional and integral gains. The quotient C/B represents the transfer function to be controlled, where B and C are presently defined as follows :

$$B = L_s R_r + s.L_r L_s \sigma \text{ and } C = MV_s \tag{27}$$

The regulator terms are calculated with a pole compensation method [19]. The time response of the controlled system will be fixed at 10 ms. This value is sufficient for our application and a lower value might involve transients with important overshoots. The calculated terms are :

$$K_i = \frac{1}{10^{-3}} \frac{L_s R_r}{MV_s} \tag{28}$$

$$K_p = \frac{1}{10^{-3}} \frac{L_s L_r \sigma}{MV_s} \tag{29}$$

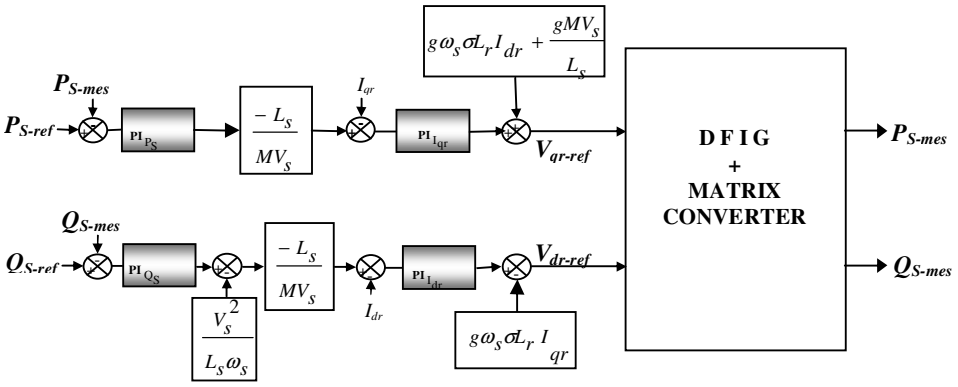

Fig. 4. Block diagram of power control by PI.

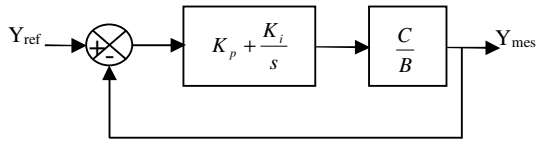

Fig. 5. System with PI controller.

It is important to specify that the pole-compensation is not the only method to calculate a PI controller but it is simple to elaborate with a first-order transfer-function and it is sufficient in our case to compare with other controllers. This synthesis method is also used to determine the current loops corrector's parameters.

6. SOSMC design

The first order sliding mode control (SMC) is an effective nonlinear robust control. However, a few problems arise in some practical applications, such as chattering effect and undesirable mechanical stresses. The second order sliding mode algorithm synthesizes a discontinuous control which makes the surface and its derivative null with continuous control, therefore reducing chattering and avoiding strong mechanical efforts while preserving (SMC) advantages [20]. The block diagram of the second order sliding mode control applied to the DFIG is illustrated in Figure 6. Let us consider the following surfaces:

$$\begin{cases} e_d = Q_s - Q_{s\,ref} \\ e_q = P_s - P_{s\,ref} \end{cases} \tag{30}$$

We derived the above errors, we obtain:

$$\begin{cases} \dot{e}_d = \dot{Q}_s - \dot{Q}_{s\,ref} \\ \dot{e}_q = \dot{P}_s - \dot{P}_{s\,ref} \end{cases} \tag{31}$$

Expressions of active and reactive power by his expressions expressed in equation (24) is replaced, we obtain:

$$\begin{cases} \dot{e}_d = \dfrac{-V_s M}{L_s}\dot{I}_{dr} - \dot{Q}_{s\,ref} \\ \dot{e}_q = \dfrac{-V_s M}{L_s}\dot{I}_{qr} - \dot{P}_{s\,ref} \end{cases} \tag{32}$$

Posing A such that: $A = \dfrac{-V_s M}{L_s}$

Expressions of direct and quadrate rotor currents of equation (25) are replaced in equation (32) yields:

$$\begin{cases} \dot{e}_d = \dfrac{A}{\sigma L_r}[V_{dr} - R_r I_{dr} + g\omega_s\sigma L_r I_{qr}] - \dot{Q}_{s\,ref} \\ \dot{e}_q = \dfrac{A}{\sigma L_r}[V_{qr} - R_r I_{qr} - g\omega_s\sigma L_r I_{dr} - g\dfrac{MV_s}{L_s}] - \dot{P}_{s\,ref} \end{cases} \tag{33}$$

Equation (33) can be written:

$$\begin{cases} \dot{e}_d = \dfrac{A}{\sigma L_r}V_{dr} + \dfrac{A}{\sigma L_r}[-R_r I_{dr} + g\omega_s\sigma L_r I_{qr}] \\ \qquad\qquad - \dot{Q}_{s\,ref} \\ \dot{e}_q = \dfrac{A}{\sigma L_r}V_{qr} + \dfrac{A}{\sigma L_r}[-R_r I_{qr} - g\omega_s\sigma L_r I_{dr} - g\dfrac{MV_s}{L_s}] \\ \qquad\qquad - \dot{P}_{s\,ref} \end{cases} \tag{34}$$

Posing G1 and G2 such that:

$$\begin{cases} G_1 = \dfrac{A}{\sigma L_r}[-R_r I_{dr} + g\omega_s\sigma L_r I_{qr}] - \dot{Q}_{s\,ref} \\ G_2 = \dfrac{A}{\sigma L_r}[-R_r I_{qr} - g\omega_s\sigma L_r I_{dr} - g\dfrac{MV_s}{L_s}] - \dot{P}_{s\,ref} \end{cases} \tag{35}$$

Then it follows that:

$$\begin{cases} \dot{e}_d = \dfrac{A}{\sigma L_r} V_{dr} + G_1 \\ \dot{e}_q = \dfrac{A}{\sigma L_r} V_{qr} + G_2 \end{cases} \tag{36}$$

On deriving the relationship of equations (36) yields:

$$\begin{cases} \ddot{e}_d = \dfrac{A}{\sigma L_r} \dot{V}_{dr} + \dot{G}_1 \\ \ddot{e}_q = \dfrac{A}{\sigma L_r} \dot{V}_{qr} + \dot{G}_2 \end{cases} \tag{37}$$

The SOSMC proposed based on the super twisting algorithm known (ST) which is introduced by Levant [21].

$$V_{dr} = u_1 + u_2 \tag{38}$$

Then it follows that:

$$\begin{cases} \dot{u}_1 = -\alpha_1 \, sign(e_d) \\ u_2 = -\theta_1 \left| e_d \right|^{0.5} sign(e_d) \end{cases} \tag{39}$$

And:

$$V_{qr} = w_1 + w_2 \tag{40}$$

Including:

$$\begin{cases} \dot{w}_1 = -\alpha_2 \, sign\,(e_q) \\ w_2 = -\theta_2 \left| e_q \right|^{0.5} sign\,(e_q) \end{cases} \tag{41}$$

To ensure the convergence of controllers in the infinity of time constants α_i and θ_i are chosen to satisfy the following inequality:

$$\begin{cases} \alpha_i > \dfrac{\mu_i}{\sigma L_r} \\ \theta_i \geq \dfrac{4\mu_i(\alpha_i + \mu_i)}{\sigma^2 L_r^2 (\alpha_i - \mu_i)} \\ \left| \dot{G}_i \right| < \mu_i \;;\; i = 1 \,,\; 2 \end{cases} \tag{42}$$

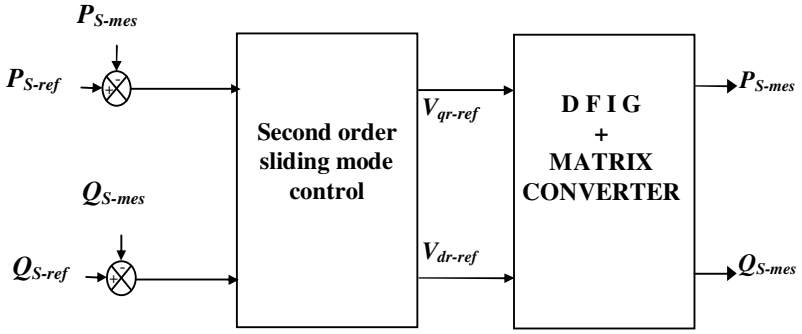

Fig. 6. Block diagram of power control by SOSMC.

7. DFIG-grid synchronization process

A specific methodology needs to be adopted for effective synchronization. So far we described one of the stages of synchronization which was to generate stator induced voltage identical in magnitude, phase angle and frequency to the grid voltage. The second stage of synchronization process involves precise control of the three-phase circuit breaker which is the interconnecting bridge between the power grid and the stator of the DFIG. The start-up and synchronization process irrespective of the type of orientation frame used can be achieved in steps mentioned below [22,23,24].

A. Turbine acceleration

The first step is to start the DFIG system. The aerodynamic drive torque exerted by wind on the DRWT blades rotates the system and accelerates the generator shaft. The pitch angle β is maintained at the lowest point in order to obtain maximum torque and to keep the acceleration time very short. Due to inertia of heavy masses of the dual rotor wind turbine mechanical system, this step can take the longest time.

B. Controller initialization

As the DRWT speeds up to the cut-in wind speed, the rotor-side current controller is initialized. The *d-q* rotor control voltage generated by the controller is injected to the rotor of the DFIG through the matrix converter to induce voltage in the stator. The voltage induced in the

stator is produced. At this stage, the stator is ready to be connected to the power grid. However step C ahead needs to be understood before making connection by closing the circuit breaker.

C. Stator connection

This is the most critical stage of the synchronization process. The time at which the three-phase circuit breaker needs to be closed for connecting the stator is very important. Care has to be taken that the breaker is closed at a point of time when the stator induced voltage is exactly equal in magnitude to the grid voltage. The stator induced voltage would be in phase with grid voltage and so would be the frequency, but the magnitude needs to be monitored. If the circuit breaker is closed with a stator induced voltage less than the grid voltage, heavy transient stator and rotor currents would be observed which indicates unsuccessful synchronization.

In general, these conditions can be summarized in form of equations given below.

$$V_{grid}\sin(\omega_{grid}\,t+\varphi)=V_{stator}\sin(\omega_{stator}\,t+\varphi) \quad (43)$$

$$\left|V_{grid}\right|=\left|V_{stator}\right| \text{ and } f_{grid}=f_{stator} \quad (44)$$

Where φ_{grid}, φ_{stator}, V_{grid}, V_{stator}, f_{grid}, f_{stator}, $|V_{grid}|$, $|V_{stator}|$ are the phase angle, peak value, frequency and magnitude of the grid and stator voltage respectively.

8. Simulation results and discussions

In this section, simulations are realized with a 1.5 MW generator coupled to a 398V/50Hz grid, fed by a matrix converter and driven by dual rotor wind turbine. The system parameters are given next in appendix. The whole system is simulated using the Matlab / Simulink software.

In the objective to evaluate the performances of the controllers, six categories of tests have been realized: extracted mechanical power of DRWT and SRWT, stator-grid synchronization, pursuit test, comparison between the waveforms of the statoric currents using the SMC and SOSMC, sensitivity to the speed variation and robustness facing variations of the machine's parameters.

A. Extracted mechanical power

Figure 7 shows a comparison of mechanical power extracted from a single and dual rotor wind turbine. The mechanical power extracted at time t = 50 s of SRWT is equal to 0.536 MW and the power of the DRWT equal to 0.642 MW.

From this simulation result, we note that the mechanical power of the dual rotor wind turbine has increased by about 20% compared to that of single-rotor wind turbine.

B. Stator-grid synchronization

Figure 8 shows the stator connection for one of the three phase voltages. The fundamental component of the stator induced voltage (V_{stator}) over the grid voltage (V_{grid}) shows no deviation in magnitude, phase angle and frequency. A high frequency noise is observed in the induced voltage before the synchronization (t = 0.02s). We can conclude that, A successful synchronization at t = 0.02s reflects in almost no or very low impact on the grid.

C. Pursuit test

This test has for goal the study of the two controller's behaviours in reference tracking, while the machine's speed is considered constant at its nominal value. The simulation results are presented in figure 9. As it's shown by this figure, for the two controllers, the active and reactive generated powers tracks almost perfectly their references.

In addition and contrary to the PI controller where the coupling effect between the two axes is very clear, we can notice that the SOSMC controller ensures a perfect decoupling between them. Therefore we can consider that the second order sliding mode controller has a very good performance for this test.

D. Waveforms of the statoric currents

Figure 10 and 11 shows the waveforms of the statoric currents and their total harmonic distortion (THD) using the SMC and SOSMC. It can be clear observed that the THD is reduced for SOSMC (THD = 2.62%) when compared to SMC (THD = 3.13%).

Therefore it can be concluded that the proposed controller (SOSMC) is the most effective in eliminating chattering phenomenon.

E. Sensitivity to the speed variation

The aim of this test is to analyze the influence of a speed variation of the DFIG on active and reactive powers. For this objective and at time = 0.02s, the speed was varied from 150 rad/s to 100 rad/s. The simulation results are shown in figure 12.This figure express that the speed variation produced an important oscillations on the powers curves of the system with PI controller, while the effect is almost negligible for the system with SOSMC one. We can notice that this last has a nearly perfect speed disturbance rejection, indeed; only very small power variations can be observed (fewer than 3%). This result is attractive for wind energy applications to ensure stability and quality of the generated power when the speed is varying.

F. Robustness

In order to test the robustness of the used controllers, the machines' parameters have been intentionally modified with overkill variations: the values of the stator and the rotor resistances R_s and R_r are doubled and the values of inductances L_s, L_r and M are divided by 2. The machine is running at its nominal speed. The gotten results are represented on figure 13.

These results show that parameters variations of the DFIG present a clear effect on the powers curves and that the effect proves more significant for PI controller than that with SOSMC. This result enables us to conclude that this last controller (SOSMC) is more robust.

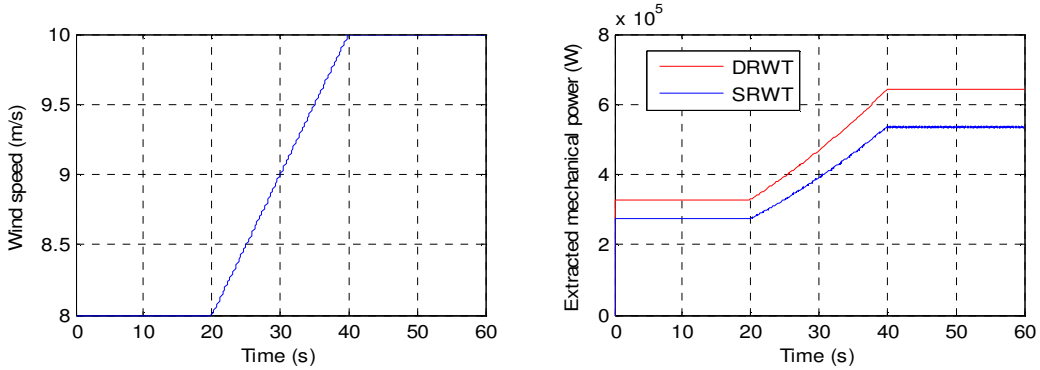

Fig. 7. Comparison of extracted mechanical power between the SRWT and DRWT.

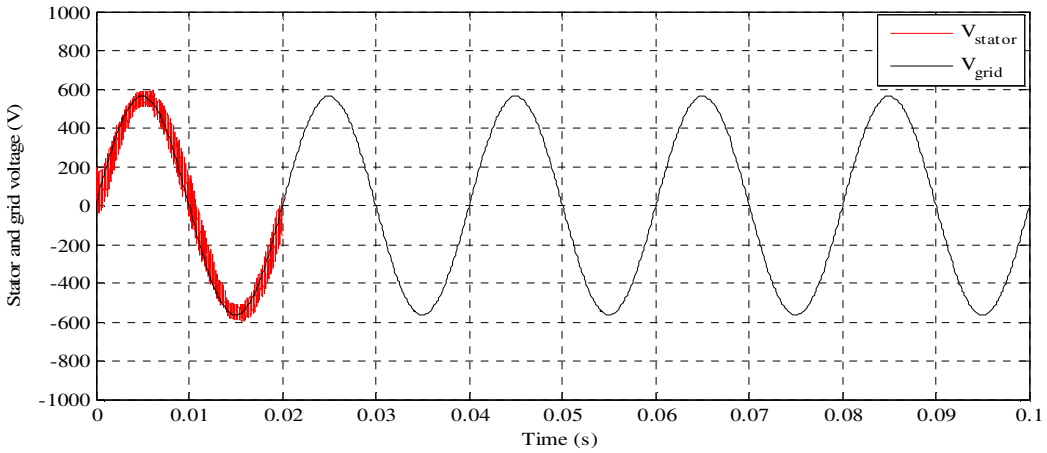

Fig. 8. Stator-grid synchronization.

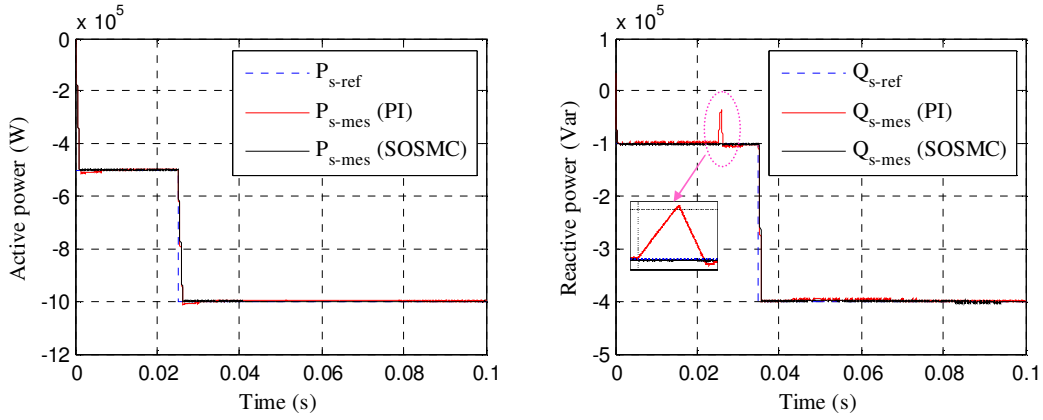

Fig. 9. Comparison result between the PI controller and SOSMC (Pursuit Test).

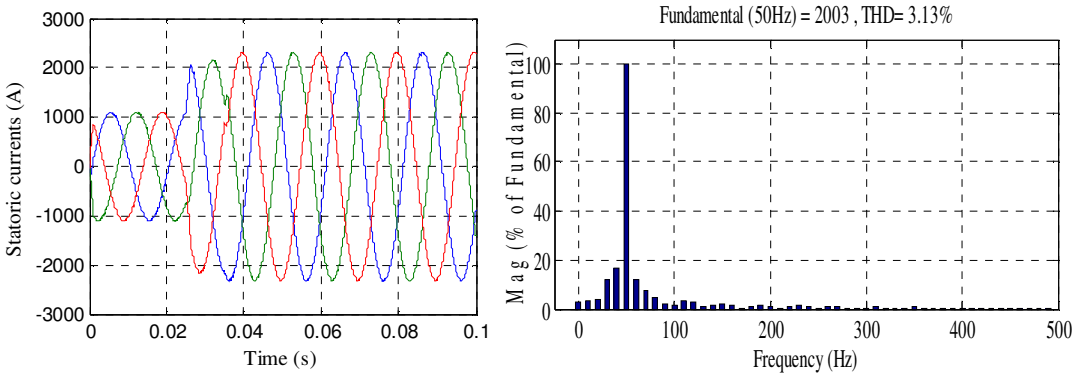

Fig. 10. Waveforms of the statoric currents and their THD with the SMC.

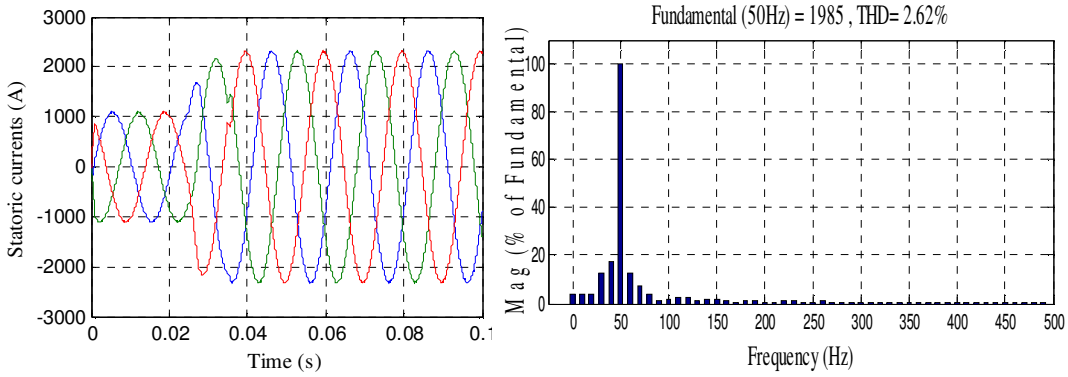

Fig. 11. Waveforms of the statoric currents and their THD with the SOSMC.

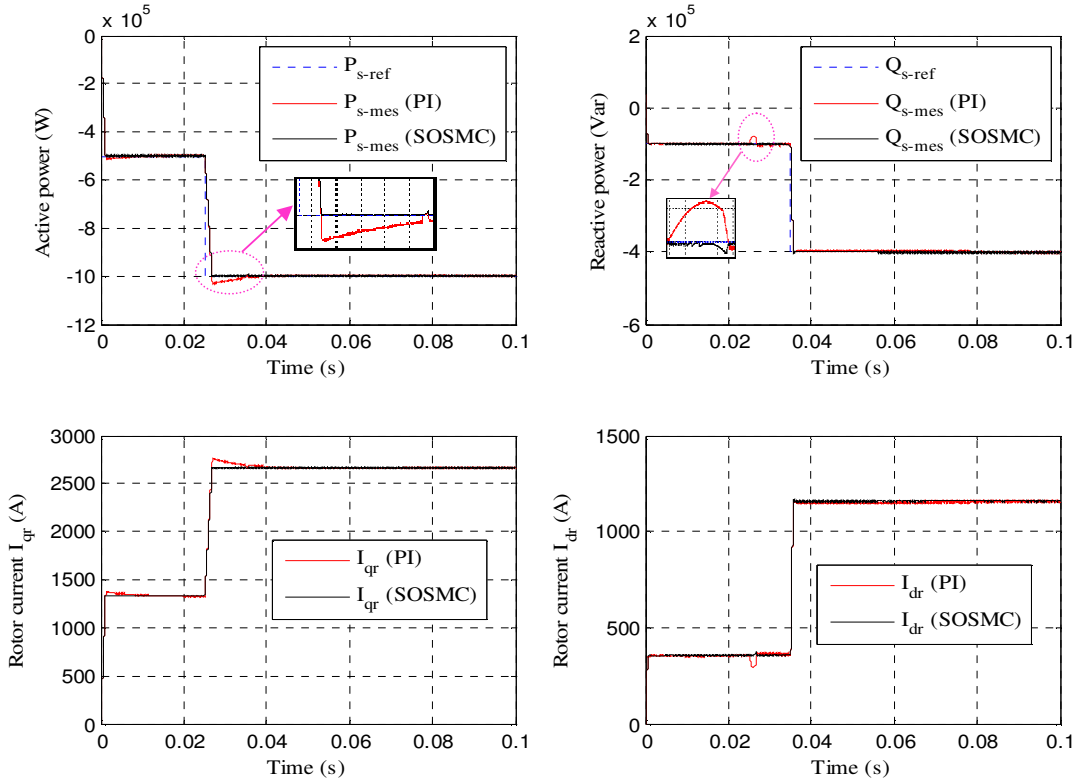

Fig. 12. Sensitivity to the speed variation.

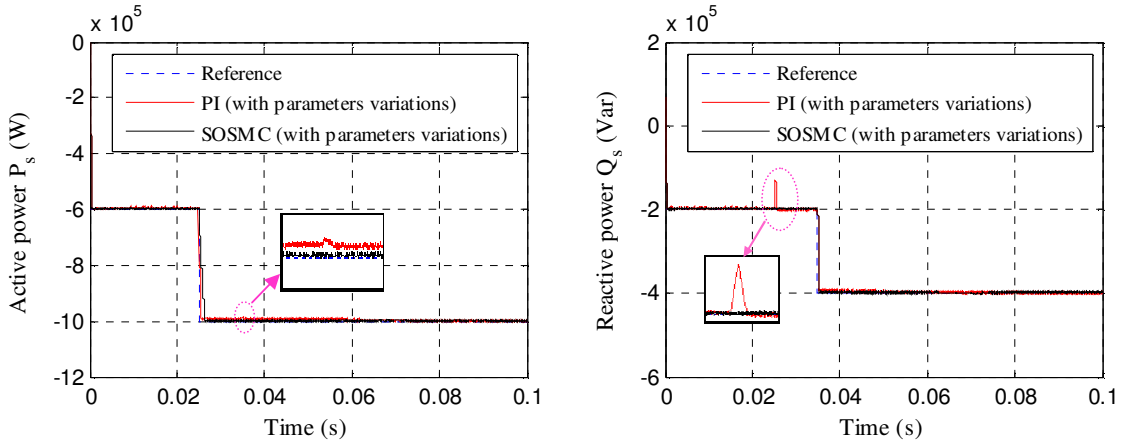

Fig. 13. Sensitivity to the machine's parameters variations on the DFIG control.

9. Conclusion

The modeling, the control and the simulation of an electrical power based on a doubly fed induction generator driven by DRWT, connected directly to the grid by the stator and fed by a matrix converter on the rotor side has been presented in this study.

Our objective was the comparison of extracted mechanical power between the single and dual rotor wind turbine, we note that the mechanical power of the dual rotor wind turbine has increased by about 20% compared to that of single-rotor wind turbine.

The implementation of a robust decoupled control system of active and reactive powers generated by the stator side of the DFIG, in order to ensure of the high performance and a better execution of the DFIG, and to make the system insensible with the external disturbances and the parametric variations. In the first step, we started with a study of modeling on the DRWT. Second step, we study the matrix converter modeling controlled by the Venturini modulation technique, because this later present a reduced harmonic rate and the possibility of operation of the converter at the input unit power factor. In third step, we adopted a vector control strategy in order to control statoric active and reactive power exchanged between the DFIG and the grid. In the final step, two different controllers are synthesized and compared. In term of power reference tracking with the DFIG in ideal conditions, the SOSMC ensures a perfect decoupling between the two axes comparatively to the PI controller where the coupling effect between them is very clear. When the machine's speed is modified, the impact on the active and reactive powers values is important for PI controller whereas it is almost negligible for SOSMC one. A robustness test has also been investigated where the machine's parameters have been modified. These changes induce some disturbances on the powers responses but with an effect almost doubled with the PI controller than on that with SOSMC one. Basing on all these results we conclude that robust control method as SOSMC can be a very attractive solution for devices using DFIG such as wind energy conversion systems.

Appendix

Table 1
DRWT parameters

Parameters	Rated Value	Unity
Power of DRWT	1.5	MW
Main rotor diameter	51	m
Auxiliary rotor diameter	26.4	m

Table 2
DFIG parameters

Parameters	Rated Value	Unity
Stator voltage	398	V
Stator frequency	50	Hz
Number of pairs poles	2	
Nominal speed	150	rad/s
Stator resistance	0.012	Ω
Rotor resistance	0.021	Ω
Stator inductance	0.0137	H
Rotor inductance	0.0136	H
Mutual inductance	0.0135	H

References

1. Seungmin, L., Eunkuk, S., Soogab, L.: *Velocity interference in the rear rotor of a counter-rotating wind turbine*. In: Renewable Energy xxx (2012) 1-6, 2012.
2. Hau, E.: *Wind turbines-fundamentals, technologies, application, economics*. In: 2nd ed. Berlin, Springer, 2006.
3. Newman, BG.: *Actuator-disc theory for vertical-axis wind turbines*. In: Journal of Wind Engineering and Industrial Aerodynamics 1983, 15:347e55.
4. Manwell, J.F., McGowan, J.G, Rogers, A.L.: *Wind Energy Explained, Theory, Design and Application*. In: John Wiley & Sons Ltd., 2002, pp. 84–88.
5. Levant, A.: *Sliding order and sliding accuracy in sliding mode control*. In: Int. J. Control, vol. 58, pp. 1247–1263,

1993.
6. Emelyanov, S., Korovin, S., Levant, A.: *High-order sliding modes in control systems*. In: Computational mathematics and modelling, vol. 7, no. 3, pp. 294–318, 1996.
7. Bartolini, G., Ferrara, A., Usai, E.: *Output tracking control of uncertain nonlinear second-order systems*. In: Automatica, vol. 33, no. 12, pp. 2203–2212, 1997.
8. Utkin, V. I.: *Sliding Modes in Control and Optimization*. In: Springer Verlag, 1992.
9. Bartolini, G., Ferrara, A., Usai, E.: *On second order sliding mode controllers, in Variable Structure Systems, Sliding Mode and Nonlinear Control*. In: ser. Lecture Notes in Control and Information Sciences, K. Young and U. Ozguner, Eds. Springer Verlag, 1999.
10. Levant, A.: *Controlling output variables via higher order sliding modes*. In: Proc. of the European Control Conference, ECC'99, Karlsruhe, Germany, 1999.
11. Laghrouche, S., Plestan, F., Glumineau, A.: *Higher order sliding mode control based on optimal linear quadratic control*. In: Proc. of the European Control Conference, ECC'03, Cambridge, England, 2003.
12. Elisabetta, P.: *MIMO Second Order Sliding Mode Control*. In: IEEE International Workshop on Variable Structure Systems Alghero, Italy, June 5-7, 2006.
13. Farahani, E.M, Hosseinzadeh, N., Ektesabi, M. M.: *Comparison of Dynamic Responses of Dual and Single Rotor Wind turbines under Transient Conditions*. In: IEEE ICSET Siri Lanka Kandy 2010.
14. No, T.S., Kim b, J.E., Moon, J.H., Kim c, S.J.: *Modeling , control, and simulation of dual rotor wind turbine generator system*. In: Renewable Energy 34 (2009) 2124-2132, 2009.
15. Boudjema, Z., Meroufel, A., Bounadja, A., Djeriri, Y.: *Nonlinear control of a doubly fed induction generator supplied by a matrix converter for wind energy conversion systems*. In: journal of electrical engineering, Vol. 13, No 4, pp.269-276, 2013.
16. Cupertino, F., Naso, D., Mininno, E., Turchiano, B.: *Sliding-mode control with double boundary layer for robust compensation of payload mass and friction in linear motors*. In: IEEE Trans. On Industry Applications, Vol. 45, No. 5, pp. 1688-1696, Sep./Oct 2009.
17. Chikha, S., Barra, K., Reama, A.: *Predictive current control of a wind energy conversion system based DFIG via direct matrix converter*. In Proc. of IEEE IREC 2015, pp. 1-7, 24-26 March 2015.
18. Venturini, M.: *A new sine wave in sine wave out conversion technique which eliminates reactive elements*, In: Proc Powercon 7, San Diego, CA, pp E3-1, E3-15, 27-24 March 1980.
19. Boyette, A. : *Contrôle–commande d'un générateur asynchrone à double alimentation avec système de stockage pour la production éolienne*. In : PhD Thesis, University of Nancy I, France, 2006.
20. Abdeddaim, S., Betka, A.: *Optimal tracking and robust power control of the DFIG wind turbine*. In: Electrical Power and Energy Systems 49 (2013) 234-242.
21. Levant, A.: *Integral high -order sliding modes*. In: IEEE Trans, Automatic Control, vol. 52, No. 7, pp. 1278-1282, July 2007.
22. Ghandehari, R., Zeinolabedin, M., Ghaffari, N.: *DFIG Grid-Synchronization Control of a WECS Based on a Matrix Converter*. In: IRACST – Engineering Science and Technology: An International Journal (ESTIJ), ISSN: 2250-3498, Vol.2, No. 3, June 2012.
23. Wong, K. C., Ho, S. L., Cheng, K. W. E.: *Direct voltage control for grid synchronization of doubly-fed induction generators*. In: Electr. Power Compon. Syst., vol. 36, no. 9, pp. 960–976, Sep. 2008.
24. Munteanu, I., Bacha, S., Bratcu, A., Guiraud , J., and Roye, D.: *Energy reliability optimization of wind energy conversion systems by sliding mode control*. In: IEEE Trans. Energy Convers, vol. 23, no. 3, pp. 975–985, Sep. 2008.